Foaming of a Polymer–Nanoparticle System: Effect of the Particle Properties

M. H. N. Famili, Hamed Janani, M. S. Enayati

Department of Polymer Engineering, Tarbiat Modares University, P.O. Box 14115-143, Tehran, Iran

ABSTRACT: This work is an experimental study of the effects of nanoparticles with different characteristics and contents on foaming composites made of three different nanosilica particles with different geometrical and chemical surface properties in a polystyrene matrix. In addition to the general characteristics reported in our last study on the morphology of polymer–nanoparticle composites, this study shows that nanosilicas of larger sizes can result in foams of higher cell densities. Additionally, the cell densities of foams can be reduced if the nanoparticle surface becomes more affine to the polymer matrix chemically. These results show a correspondence with the effects of the characteristics of the nucleation agent on the nucleation of bubbles, which have been explored previously. © 2010 Wiley Periodicals, Inc. J Appl Polym Sci 119: 2847–2856, 2011

Key words: blowing agents; nanocomposites; nucleation; particle nucleation; polystyrene

INTRODUCTION

Many efforts have been made to modify the microcellular foaming process to increase the cell density and decrease the cell size. Rapid pressure quenching during the foaming of polymers with high levels of interaction with carbon dioxide (CO_2) as a blowing agent at low temperatures and high pressures along with the use of retrograde vitrification,[1] the foaming of polymers with high glass-transition temperatures,[2] polymer blending,[3] and the use of nanoparticles in the polymer matrix[4–13] are examples of these efforts. The inducement of nanocellular structures in polymers due to the unique and superior mechanical and physical properties expected from nanofoams is the main motivation for this research. There are few studies about the creation of nanocellular structures in polymers,[14–19] so nanofoam production techniques are very limited and special. The major drawback of these studies is the fact that the processing conditions (e.g., the temperature ranges) presented in these studies are not comparable to those of conventional industrial polymer processes such as extrusion and injection molding. Therefore, the direct use of the results in conventional polymer processes is rather limited.

The top–down approach to nanotechnology signifies the modification of microscale processing techniques to produce nanoscale features.[4] In our previous research,[20] we thus performed a set of microcellular foaming experiments and used a defined strategy to control the cell structure and produce polymeric foams with novel structures. The backbone of our foaming strategy (the process and experiments) is based on increasing the nucleation rate of bubbles in the foaming process. This means controlling the foaming process in such a way that after rapid thermodynamic instability, much of the blowing agent dissolved in the polymer is separated for the nucleation of large numbers of fine bubbles. In this point of view, to produce foam structure with nano-scale features, it is necessary to obtain required process conditions (i.e. temperature and saturation pressure) for production of large numbers of nanosized nuclei as well as controlled stabilization of the obtained cellular structure.

There are many studies in the literature reporting the effects of the addition of nanoparticles to the polymer matrix on the cell density of the resultant foams.[4–14] In this study, we followed the effects of the addition of nanosilica on the nucleation and the final foam structure. We found that the presence of these added surfaces could lead to control of the nucleation sites and thus the structure of the final foam.

We need to obtain thorough knowledge of the foaming of three-component systems (polymer, supercritical fluid, and nanoparticles) to be able to adjust the specific characteristics of the components to obtain the desired foam structures. This is preferable to controlling processing conditions such as the temperature, pressure, pressure drop rate, and stabilization of the cellular structure, which may be more difficult.

There are several parameters that could affect the morphology of nanocomposite foams. By adding nanoparticles, we in fact introduce some surfaces to the basic homogeneous polymer/supercritical solution. This can alter the phase-separation phenomenon, which occurs after spontaneous thermodynamic instability. One part of this influence is related to the quantity and quality of such surfaces, which are expressed in terms of the particle content and the quality of the particle distribution and dispersion in the matrix, and they determine the number of centers potentially available for nucleation. Previously reported observations[4–14] on the increasing effect of inserted surfaces on the cell density of foams are thought to be due to the manipulation of the nucleation phenomenon. Therefore, it is important for these surfaces to become favorite spots for the nucleation of gas bubbles. According to classical nucleation theory, the geometrical and chemical characteristics of surfaces determine how much they energetically favor the nucleation of gas bubbles.

In this study, we have explored the effects of the geometrical and chemical characteristics of nanosilica surfaces on the structure of foams through adjustments of the contents of these surfaces in the polymer matrix. In the remainder of this work, we first present an overview of the previous studies on the effects of the nanoparticle content, distribution, and dispersion on the morphology of the produced foams. Next, we continue our review with a focus on the effects of surface properties of nanoparticles. Then, we use classical nucleation theory to describe the effects of such surfaces through adjustments of characteristic parameters, and we state the experimental features of the study. Finally, the results are presented and discussed.

Effects of the presence of nanoparticles

To control the foam morphology and the inducement of desired cell structures, one conventional practice is the use of additives as nucleating agents. In their pioneering efforts, Colton and Suh[21,22] sought to elucidate the mechanism of nucleation in bicomponent thermoplastic foams such as polystyrene modified by zinc stearate. Their results have revealed that a substantial increase in the pore cell population can be achieved through the incorporation of a small amount of an additive (at a concentration level below its solubility limit) in combination with a high saturation pressure of the blowing agent. These effects are synergistic, in that they lower the interfacial tension and intermolecular potential energy and thereby reduce the activation energy barrier for nucleation and increase the number of small pore cells.[21,22]

Siripurapu et al.[6] considered the inducement of nanosurfaces in a polymer matrix by spherical silica nanoparticles. Colloidal nanosilica particles inherently possess a negative double-layer charge on their surface, so they do not tend to agglomerate.[6] Increasing the nanosilica content increases the cell density at certain temperatures and pressures. This observation is more common at lower pressures and temperatures because heterogeneous nucleation is the dominant nucleation mechanism under these conditions. Furthermore, nanoparticles have significant effects on the stabilization of nucleated bubbles, especially at high temperatures.[6]

Studies such as these provide fundamental insight into the role of heterogeneous nucleation in polymer foaming. Any characteristic aspects of composites, such as the filler content and the dispersion and distribution of particles, could affect the final morphology of foamed composites.

Foams with finer fillers have higher cell densities at high saturation pressures.[5] A fine dispersion of these nucleation agents can facilitate the formation of nucleation centers for a gaseous phase. Polymer nanocomposite foams exhibit substantially improved physical and mechanical properties versus their neat polymer foam counterparts.[11,12]

The amount and distribution of the nucleation agents are also important factors for determining the foam quality.[5] The cell density is determined by the concentration of the foaming agent. A nonuniform distribution of the nucleation agents results in a foam that has more cells in the agent-rich area and fewer cells in the agent-deficient areas; this leads to a nonuniform cell size distribution in the foam product.[5] The effect of the particle concentration on foam nucleation has been previously investigated.[12,13] The cell density increases linearly versus the nanoparticle concentration at low concentrations.[13]

The effect of the clay nanoparticle dispersion on the foam cell morphology has been studied in detail.[10,11] Both intercalated and exfoliated polystyrene–clay nanocomposites have been synthesized via *in situ* polymerization. Exfoliated nanocomposites have yielded much higher nucleation rates than intercalated nanocomposites. This has been attributed to the fact that even with the same nominal particle concentration; the effectiveness of the particle concentration is higher once the particles are better dispersed. Hence, more heterogeneous nucleation sites are available.[11]

As mentioned before, these characteristics (i.e., the particle content, distribution, and dispersion) directly determine the number of available nucleation sites and their distribution.

Effects of the surface properties

Nanoparticles, in comparison with conventional micrometer-sized filler particles, have greater specific surface

areas. Therefore, a significantly higher effective particle concentration can be achieved at a low nominal particle concentration.[4] Both could lead to improved nucleation efficiency.[4]

The surface properties of nanoparticles include geometrical properties, such as the particle shape, size, and size distribution. There are few reports on the effects of the geometry of particles on foaming efficiency.[23–25] Shen et al.[23] compared the nucleation efficiency of carbon nanofibers, single-walled carbon nanotubes, and nanoclays. They demonstrated that, in comparison with nanoclay and single-walled carbon nanotubes, carbon nanofibers exhibited substantially higher nucleation efficiency.[23] They stated that this was due to their good dispersion in the polymer matrix as well as the favorable wettability and surface curvature in the foaming process.[23]

There are also some studies on the effect of the chemistry of nanoparticles[4,10,24,26] and especially nanosilica particles.[24] The surface chemistry of clay nanoparticles not only affects the particle dispersion but also has a pronounced effect on the nucleation efficiency in a polymer–clay foaming agent system.[4] The chemical nature of the polymeric chain, which is tethered to the surface of the nanoclay, has the same effect.[10] The importance of both is due to the significance of the typical interaction of the foaming agent with the interfacial region between the polymer and nanoclay because the nanoparticle surface chemistry and the polymer chain directly determines the quality of this interaction. Additionally, the ability of particles to act as nucleation sites is determined by the degree of bonding between the particles and polymer.[27] If there is a high degree of bonding, a large amount of energy will be required to force the interface apart.[27] If this energy is high enough, nucleation may be precluded. If a poor bond exists, the interface will have a large amount of energy associated with it, and this will enhance nucleation.[27]

By adjusting the interaction of supercritical CO_2 (a blowing agent) and the surface of nanoclay, Zeng et al.[10] considered the morphology of cells. Exfoliated structures of nanoclay in poly(methyl methacrylate) were prepared by *in situ* polymerization. Then, the treated nanoclay was blended with polystyrene in an extruder. This treated nanoclay showed a higher nucleation efficiency than nanoclay treated by polystyrene with one methacrylic group. They concluded that a high affinity between the carbonyl group and CO_2 could result in the reduction of the bubble–particle interfacial tension and consequently in the suppression of nucleation free energy and a significant increase in the nucleation rate.

Recently, Goren et al.[24] investigated the effects of the nanoparticle size and surface chemistry on pore nucleation in silica–poly(methyl methacrylate) nanocomposites. They showed that the fluorination of the silica nanoparticle surface improved the dispersion of the nanosilica in the polymer matrix (and thus increased the potential nucleation sites), decreased the surface energy, and led to decreased critical activation energy (because of the high affinity between CO_2 and the fluorinated surface of the nanoparticles). Both increased the nucleation rate and cell density in the final foam. They also showed that decreasing the nanosilica size at a certain weight fraction increased the cell density of the final foam because of the increased number of nucleation centers, but this reduced the nucleation efficiency.

As mentioned previously, there have been few studies on nanosilica as a nucleating agent.[6,24] To study the effects of surface properties, we designed our experiments to fix the nanosilica content of the nanocomposites in such a way that they produced the same concentration of nucleation sites. Additionally, the surface-modified nanosilica was chosen to be closer to the polymer matrix chemically. This affinity could improve the dispersion of the nanoparticles and, as a result, the number of available nucleation center. On the other hand, increasing the affinity could reduce the nucleation efficiency of each of these centers. In this study, we considered these two conflicting and competitive factors.

Theoretical considerations

It is reasonable to think that the increasing effect of nanoparticles on the cell density of the final cellular structure is due to their contribution to the nucleation phenomenon. In other words, the existence of nanoparticles emphasizes phase separation via the nucleation of gas bubbles.

According to classical nucleation theory, the steady state nucleation rate (COMP: Please see the PDF file for an italic N with a dot over it followed by the superscript "hom".) can be determined with the following equation[21]:

$$\dot{N}_{\text{hom}} \ (\text{nuclei/cm}^3) = f_0 c_0 \exp(-N_G) \qquad (1)$$

where f_0 is the frequency factor, c_0 is the number of nucleation sites per cubic centimeter of the unfoamed polymer, and N_G is a dimensionless quantity called the Gibbs number. N_G is calculated as follows:

$$N_G = \frac{16\pi\gamma_{gl}^3}{kT(\Delta P)^2} \qquad (2)$$

where k is the Boltzmann constant, T is the foaming temperature, γ_{gl} is the polymer–gas interfacial tension, and ΔP is the saturation pressure. From this
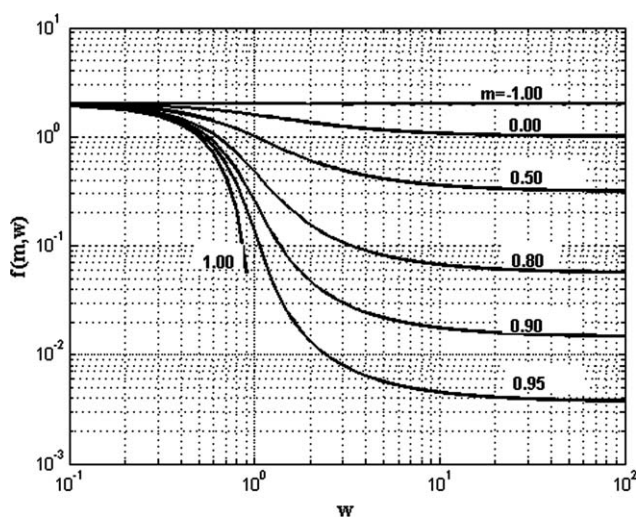
Figure 1 Gibbs free energy reduction factor (f) in terms of the relative curvature (w) and m (Cosine of the contact angle).[29]

equation, a strong dependence of the nucleation rate on T, ΔP, and γ_{gl} is evident. N_G is the most important parameter and determines the final structure of the produced foam.[28] It stands for the kinetic and thermodynamic conditions required to produce foams with specific morphological characteristics; these are independent of the foaming process, which can be batch or continuous.

In the presence of nanoparticle surfaces, N_G is affected by the Gibbs free energy reduction factor (f)[29] and N_G', Gibbs number for heterogeneous nucleation, will be:

$$N_G' = N_G \frac{f(m,w)}{2} \tag{3}$$

If $f/2$ is less than 1, the nanosurfaces facilitate the kinetic and thermodynamic conditions required to create gas bubbles. f varies as a function of the surface characteristics and specifically the contact angle and surface curvature.[29] m (Cosine of the contact angle) and the relative curvature (w) are defined as follows:

$$m = \cos \theta = \frac{\gamma_{13} - \gamma_{23}}{\gamma_{12}} \tag{4}$$

$$w = R/r_{crit} \tag{5}$$

where R is the radius of the nanoparticle, r_{crit} is the critical radius of the nuclei; θ is the contact angle between the bubble, polymer, and nanoparticles; and γ_{13}, γ_{23}, and γ_{12} are the polymer–nanoparticle, gas–nanoparticle, and polymer–gas interfacial tensions, respectively.

Figure 1 shows the functionality of the Gibbs free energy reduction factor with respect to both the surface chemistry (the contact angle) and the surface geometry (the surface curvature). Qualitatively, a small

contact angle and a large surface curvature offer a higher reduction of the critical energy and consequently an increased nucleation rate.[29] A high nucleation efficiency is obtained when the nucleant surface is energetically adequate for nucleation with respect to the corresponding homogeneous mechanism, and the nucleant is well dispersed in the polymer matrix.

Another way in which the presence of nanoparticles can affect the nucleation rate is increasing the number of nucleation sites [c_0 in eq. (1)]. The number of potential nucleation sites induced by nanoparticles can be approximately estimated as follows:

$$\frac{\text{Nucleants}}{\text{cm}^3} = \frac{wta_P}{A_P} \times \rho_{\text{blend}} \tag{6}$$

where wt is the mass fraction of the nanoparticles; ρ_{blend} is the density of the blend; and A_P and a_P are the surface area and specific surface area of the nanoparticles, respectively.
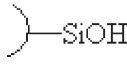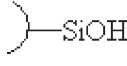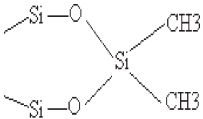
EXPERIMENTAL

Materials

General-purpose polystyrene (GP125) from Kumho Petrochemicals Co. (Seoul, Korea) was used as the polymeric matrix. Supercritical CO_2 (>%99.99) was used as the blowing agent and was purchased in solid form (dry ice) from the catering unit of Mehrabad Airport (Tehran, Iran). Nanosilicas with different characteristics (Table I) were used as fillers in the nanocomposite experiments. High-purity toluene (99%) was used as the solvent for the preparation of the nanocomposites.

Procedures

Determination of the nanoparticle content of the nanocomposites

The nanoparticle content has lower and upper physical limits. The upper limit is related to difficulties in obtaining well-dispersed nanocomposites. As mentioned earlier, for nanoparticles to play their role as nucleants more efficiently, it is necessary for them to be dispersed and distributed properly in the polymer matrix. Therefore, we fixed the weight content of the nanoparticles to be not more than 2% because higher nanoparticle contents would make dispersion more difficult[5] and rather impractical. Additionally, because of the high specific area of the nanoparticles, we expected them to have tremendous increasing effects on the cell density, even with low weight percentages. Because in heterogeneous nucleation each particle could be considered a potential nucleation site and because we were interested in producing foams with a high cell density as close as possible to a nanofoam structure (at least 10^{15} cells/

TABLE I
Characteristics of Nanosilicas

Abbreviation	Surface chemistry	Specific area (m^2/g)	Average particle size (nm)	Trade name	Company
NS_{200}	)—SiOH	200 ± 25	12	Aerosil 200	Evonic Industries
NS_{380}	)—SiOH	380 ± 30	7	Aerosil 380	Evonic Industries
NS_{150}	Si—O, Si—O, Si, CH3, CH3	150 ± 20	14	HDK H15	Wacker

cm^3),[20] the lower limit of the nanoparticle content was adjusted to provide at least this number of potential nucleation sites.

For the identification of the nanocomposites, we use PS to represent the polymer matrix (which is polystyrene), NS to represent the nanosilica, its subscript to represent the specific surface area of the nanoparticle, and N_x to represent the level of potential nucleation sites.

As mentioned before, nanoparticles not only provide sites for the nucleation of bubbles but also reduce the free energy needed for nucleation proportionally to their surface properties. Because in this study we tried to quantify the surface properties, the weight percentage of the nanoparticles in different nanocomposites was set to induce potential nucleation sites in the polymer matrix at three fixed levels. First, the nanoparticle content of PSNS$_{150}$ nanocomposites was fixed to be 1, 1.5, or 2 wt %. With eq. (6), the concentration of potential nucleation sites in each of these nanocomposites was approximated at three levels (N_1, N_2, and N_3), which are shown in Table II. The weight percentages of the nanoparticles in the PSNS$_{200}$ and PSNS$_{380}$ nanocomposites were set to induce the same level of potential nucleation sites. Table III presents in more detail nine different nanocomposites fabricated in this study.

To create well-dispersed samples but eliminate unwanted solvent bubbles, we fabricated nanocomposite master batches and employed a combination of a solution method (an efficient approach to well-dispersed nanoparticles[30]) and a melting method.

Sample preparation

General-purpose polystyrene resins were compression-molded into 0.2-mm-thick sheets at 180°C and 5000 kg/cm^2. Circular strips, 1 cm in diameter, were cut from the sheets and used for the foaming process. A combination of the solution and melting methods was used to prepare nanocomposites at different concentrations. In the first step, the nanoparticles were dispersed in the solvent at a ratio of 1 g per 100 cc of solvent with an ultrasonic mixer (UP400H, Hielscher Co. (Teltow, Germany)). Then, the suspension was mixed with a high-shear mixer at 2000 rpm for 2 h. Separately, a solution of 20 wt % polystyrene in toluene was prepared. In the next step, the specified volume of the nanoparticle suspension, calculated on the basis of the weight percentage of the nanoparticles in the final nanocomposite, was added to the polystyrene solution. The mixture was mixed further with the mixer at 2000 rpm for 12 h in a sonic bath. After that, the solvent was removed in a convection oven at 80°C for 72 h.

TABLE II
Number of Potential Nucleation Sites per Unit of Polymer Volume

	N_1	N_2	N_3
Number density of potential nucleation sites	2.53×10^{15}	3.8×10^{15}	5.07×10^{15}

TABLE III
Names and Nanoparticle Contents of the Fabricated Nanocomposites

Nanocomposite type	Nanocomposite name	Nanoparticle content (wt %)
PSNS$_{150}$	PSNS$_{150}$N$_1$	1%
	PSNS$_{150}$N$_2$	1.5%
	PSNS$_{150}$N$_3$	2%
PSNS$_{200}$	PSNS$_{200}$N$_1$	0.55%
	PSNS$_{200}$N$_2$	0.83%
	PSNS$_{200}$N$_3$	1.1%
PSNS$_{380}$	PSNS$_{380}$N$_1$	0.1%
	PSNS$_{380}$N$_2$	0.15%
	PSNS$_{380}$N$_3$	0.2%

1- High pressure- High Temperature vessel
2- Heater
3- Pressure sensor
4- Pressure gauge
5,6- High pressure high temperature ball valve
7- Thermocouple
8- Pump
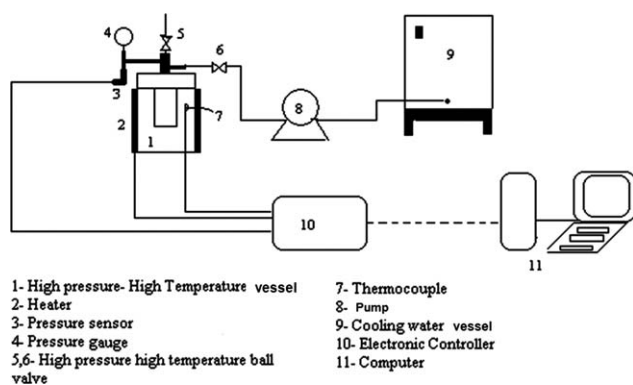9- Cooling water vessel
10- Electronic Controller
11- Computer

Figure 2 Schematic of the designed foaming process.

In the last step, to completely eliminate the solvent, the dried mixture was mixed in a Brabender internal mixer (Duisburg, Germany) at 60 rpm and 170°C for 10 min. With the same procedure described previously, the produced nanocomposites were compression-molded into 0.2-mm-thick circular sheets 1 cm in diameter.

Foaming

A novel apparatus, including a high-pressure/high-temperature vessel capable of instantaneous pressure release and controlled stabilization, was designed to foam polymers in their melt state. Figure 2 shows a schematic of this foaming apparatus. Saturation was performed under high-temperature and high-pressure conditions. The pressure drop was needed for nucleation to occur. An instantaneous pressure drop provided the required driving force for the nucleation of a sufficient number of bubbles, and with the controlled flow of cooling water into the vessel, the created morphology was stabilized. By controlling the processing conditions, we found that most of the blowing agent in the polymer matrix was used for the nucleation of bubbles, so the predominant mechanism determining the final cell structure was the controlled nucleation step.

To create foaming conditions, the vessel was pressurized with dry ice at the specified temperature. The volume of the vessel was determined precisely. The mass of dry ice required for the inducement of pressure at the specified temperature was estimated with the Peng–Robinson equation of state.

After the preparation of the foaming conditions, the sample was saturated with supercritical CO_2 for 8 h. Then, the pressure was released instantaneously ($\approx$ 300 MPa/s) with an on–off valve. The stabilization step was performed via the flow of cooling water into the vessel. Foaming was performed at 25 MPa and at 110 and 90°C to prevent other phenomena affecting nucleated bubbles, such as coalescence and gas escape from the matrix.[20]

Characterization

The density of the produced foams was measured according to ASTM D 2325.

The foamed samples were dried *in vacuo* at 50°C for 24 h, fractured in liquid nitrogen, and mounted onto stubs with carbon tape for gold sputtering in a Bal-Tec SCDOOS (Balzers, Switzerland) sputtering system. Scanning electron microscopy (SEM) pictures of the coated samples were obtained with a Philips XL30 electron microscope (Eindhoven, Netherlands). Images were acquired at an accelerating voltage of 15 kV. The images were analyzed for cell diameters and densities. The cell diameter was taken as the average of two orthogonal cell dimensions, and the cell density was calculated with the method proposed by Kumar and Suh.[31]

RESULTS AND DISCUSSION

General structural characteristics of the nanocomposite foams

Figure 3 shows SEM micrographs of the $PSNS_{200}$ and $PSNS_{380}$ nanocomposites and neat polystyrene foams. Table IV shows analyzed data from the SEM micrographs of these two nanocomposites. These data are averages of at least three repetitions (different micrographs of a sample were analyzed several times). General characteristics, which we reported in our last study,[20] could be clearly observed from these results. These characteristics included distinctively higher cell densities and lower cell sizes, incremental patterns of cell density with increasing surface contents, bimodal distributions of cell sizes, reduced densities of nanocomposite foams with respect to pure polystyrene foams, and decreasing patterns of foam density with increasing surface contents.

The effects of nanoparticles on the cell concentration can be described by the following ratio:

$$\text{Nucleation ratio} = N^*/N_0 \qquad (7)$$

where N^* is the nucleation density of the sample containing the nanoparticles and N_0 is the nucleation density of the unmodified control sample (neat polystyrene). Whenever possible, the nucleation ratio was taken as the average of at least three independent foaming experiments for that particular nanocomposite. This parameter was calculated and is shown in Table IV. These results indicate significant and positive effects of the presence of nanoparticles as nucleating agents on increasing the cell density. We observed that with increasing nanoparticle contents, the cell density of the final foams increased. Therefore, it could be concluded that nucleation was performed with nanosilica particles as nucleating agents, and heterogeneous nucleation was the dominant mechanism.
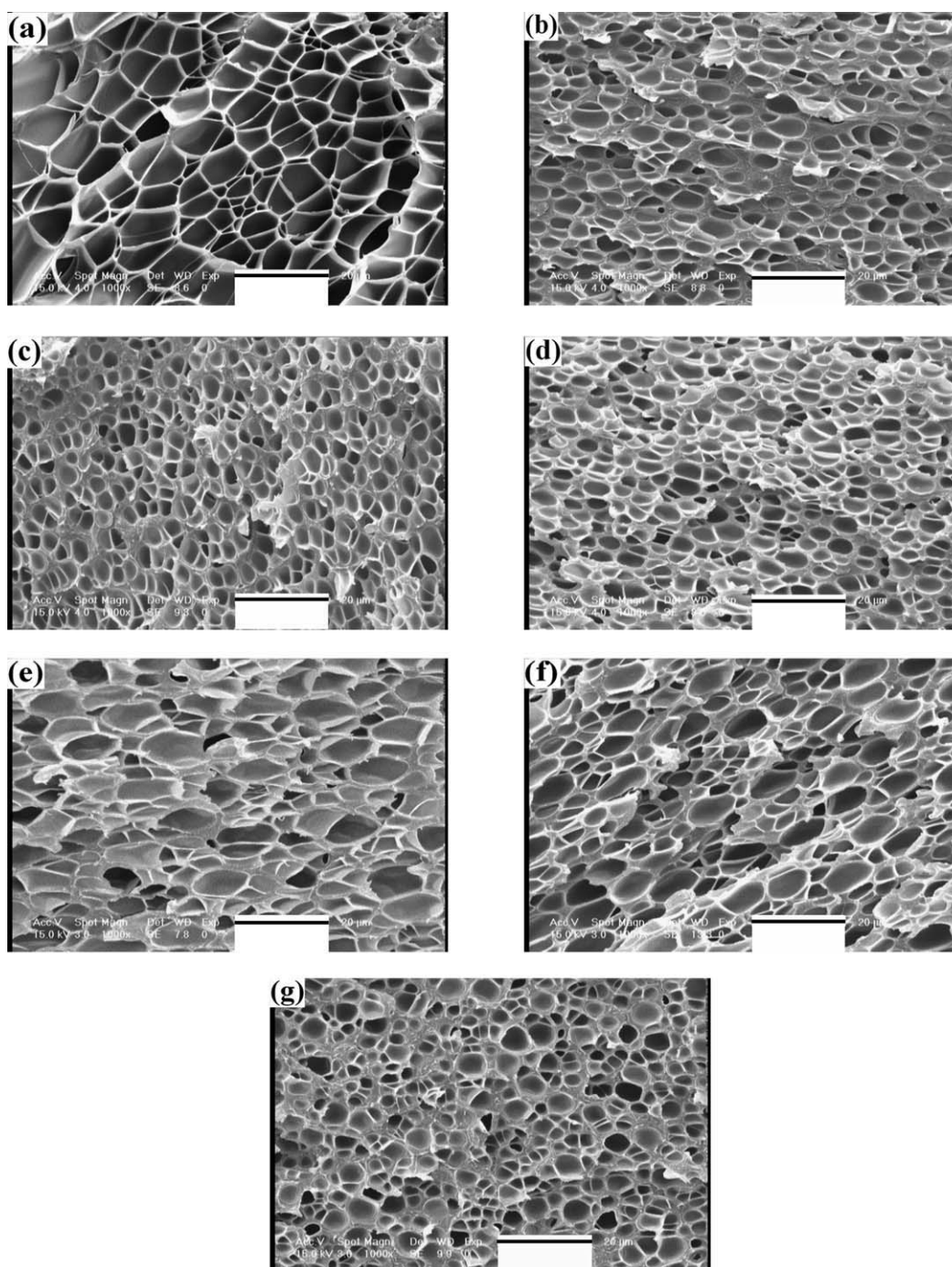
Figure 3 SEM micrographs of (a) polystyrene, (b) $PSNS_{200}N_1$, (c) $PSNS_{200}N_2$, (d) $PSNS_{200}N_3$, (e) $PSNS_{380}N_1$, (f) $PSNS_{380}N_2$, and (g) $PSNS_{380}N_3$. The scale bars are equal to 20 μm.

However, the bimodal distribution of cell sizes leads to the possibility that there are two competitive nucleation mechanisms. In fact, at higher pressures, the amount of gas absorbed in the polymer increased. This increased the rate of homogeneous nucleation, and it competed with the heterogeneous mechanism for absorbed gas.

Figure 4 shows the effect of the nanoparticle content on foam density at 90 and 110°C. The den-

sities of the nanocomposite foams were lower and decreased with increasing nanoparticle content. The reduced density of the foams with respect to unfoamed samples was due to the inducement of gas cells in the polymer matrix. The growth of bubbles near the surface of the samples punctured the surface. Hence, some of the gas that could have been used to expand the samples was vented. Figure 5 shows the holes on the surface of a foamed

TABLE IV
Cell Densities and Nucleation Ratios of the $PSNS_{200}$ and $PSNS_{380}$ Nanocomposites

Nanocomposite type	Nanocomposite name	Cell density mean (number/cm^3)	Standard deviation	Nucleation ratio[a]
$PSNS_{200}$	$PSNS_{200}N_1$	2.55×10^{11}	9.74×10^{10}	41
	$PSNS_{200}N_2$	3.49×10^{11}	1.31×10^{11}	56
	$PSNS_{200}N_3$	12.4×10^{11}	1.2×10^{11}	66
$PSNS_{380}$	$PSNS_{380}N_1$	1.50×10^{11}	1.76×10^{10}	24
	$PSNS_{380}N_2$	1.91×10^{11}	6.60×10^9	30
	$PSNS_{380}N_3$	04.2×10^{11}	1.59×10^{10}	32

[a] N_0 was 6.2×10^9.

sample of pure polystyrene. It seems that the presence of nanoparticles reduced these holes by increasing the strength of the molten polymer. The reduction of surface holes resulted in a reduction of the amount of vented gas and consequently a reduction of the density of the nanocomposite foams versus the virgin polystyrene foams.

A comparison of the cell densities and the calculated potential nucleation sites shows that the cell density was significantly lower. Indeed, the cell density at its highest level was only about one thousandth of the inserted potential sites. This means that effective and facilitative surfaces for the nucleation of gas bubbles were not prepared by the addition of nanosilica particles as much as it was primarily expected. This could be a result of the improper dispersion of nanosilicas in the polymer

matrix. The conglomeration of nanosilica particles reduced the concentration of nucleation sites. It is also plausible that the extremely large difference between the cell density of the final foam and the potential nucleation sites was due to the fact that the nanosilica surfaces were not energetically or kinetically favored for the nucleation of gas bubbles; that is, the Gibbs free energy reduction factor was high.

Effects of the surface properties of the nanoparticles

An interesting observation is the lower cell density of the $PSNS_{380}$ nanocomposite foams versus $PSNS_{200}$ (Table IV). As mentioned before, the nanoparticle contents for both samples were adjusted so that the number density of nucleation sites was equal (e.g., $PSNS_{380}N_1$ and $PSNS_{200}N_1$). Thus, this diversity in the cell density could be related to more favorable surfaces of NS_{200} nanoparticles for the nucleation of gas bubbles versus NS_{380}. In other words, NS_{380} nanoparticles had a lower reductive effect on the free energy barrier of nucleation.

Therefore, it could be concluded that the Gibbs free energy reduction factor, which depended on the contact angle between the polymer, gas, and
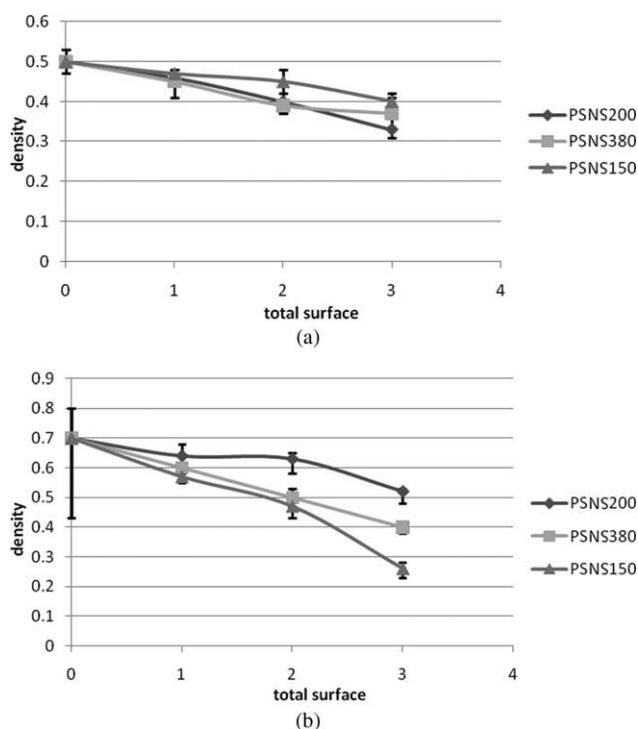

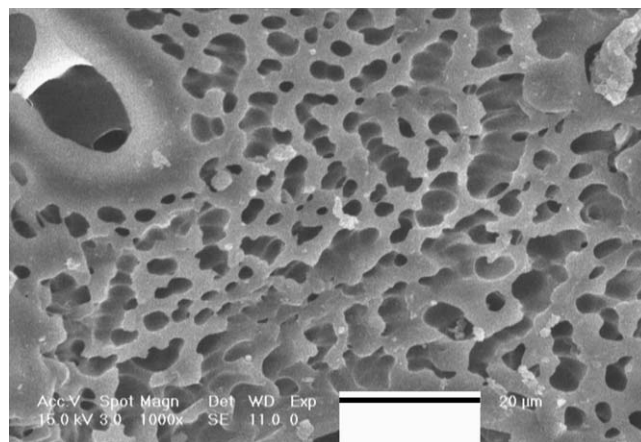**Figure 4** Densities of the nanocomposite foams at (a) 110 and (b) 90°C.

Figure 5 Holes on the surface of the pure polymer foam. The scale bar is equal to 20 μm.

nanoparticles and on the relative curvature of the surface, differed for these two types of nanocomposites. Because the chemical characteristics of the NS_{200} and NS_{380} surfaces were the same, their contact angles were the same, so the lower Gibbs free energy reduction factor for the $PSNS_{200}$ nanocomposites could be related to the larger curvature of the nucleation sites in these composites.

As previously stated, the chemistry of the nanoparticle surface determines the degree of bonding between the polymer and the particle surface, the interaction of the blowing agent with the surface of the nanoparticle, and eventually the contact angle between the polymer, gas, and nanoparticles. To explore this, $PSNS_{150}$ nanocomposites with surface-treated nanosilica were prepared and foamed for comparison with $PSNS_{200}$. Geometrically, the NS_{150} particles had a larger radius and a lower specific surface area. In the same way, the nanoparticle contents were adjusted to potentially insert the same quantity of the nucleant density at each level. Figure 6 shows SEM micrographs of these nanocomposite foams. The aforementioned general characteristics can be observed in these micrographs.

As shown in Table V, the cell density of $PSNS_{150}$ was lower than that of $PSNS_{200}$. A consideration of the results observed for the foaming of the $PSNS_{380}$ and $PSNS_{200}$ nanocomposites led us to expect that NS_{150} nanoparticles, because of their larger relative curvature under the same temperature and pressure conditions, would provide more favorable surfaces for the nucleation of gas bubbles than NS_{200} nanoparticles. In contrast, as repetitive experimental observations showed, the $PSNS_{200}$ nanocomposite foams had higher cell densities.

The lower cell densities of $PSNS_{150}$ could be related to differences in the chemical nature of the surfaces of NS_{150} and NS_{200}. The hydrophobic surface of the NS_{150} nanoparticles, which were treated with methyl groups, had a greater affinity for organic polystyrene. This high affinity led to more cohesive interactions between the polymer and particle surface. As a result, the polymer–nanoparticle interfacial tension decreased; consequently, the contact angle between the polymer, gas, and particles increased according to eq. (4). As Figure 1 shows, a higher contact angle increased the Gibbs free energy reduction factor and thus decreased the nucleation rate and depressed the cell density in the produced foam.

The noticeable point of these results is that nucleation dominates the final characteristics of the cellular structure. This can be concluded from the fact that any manipulation of the primary factors, such as the particle surface properties and content, affected the final structure in a way that could be qualitatively
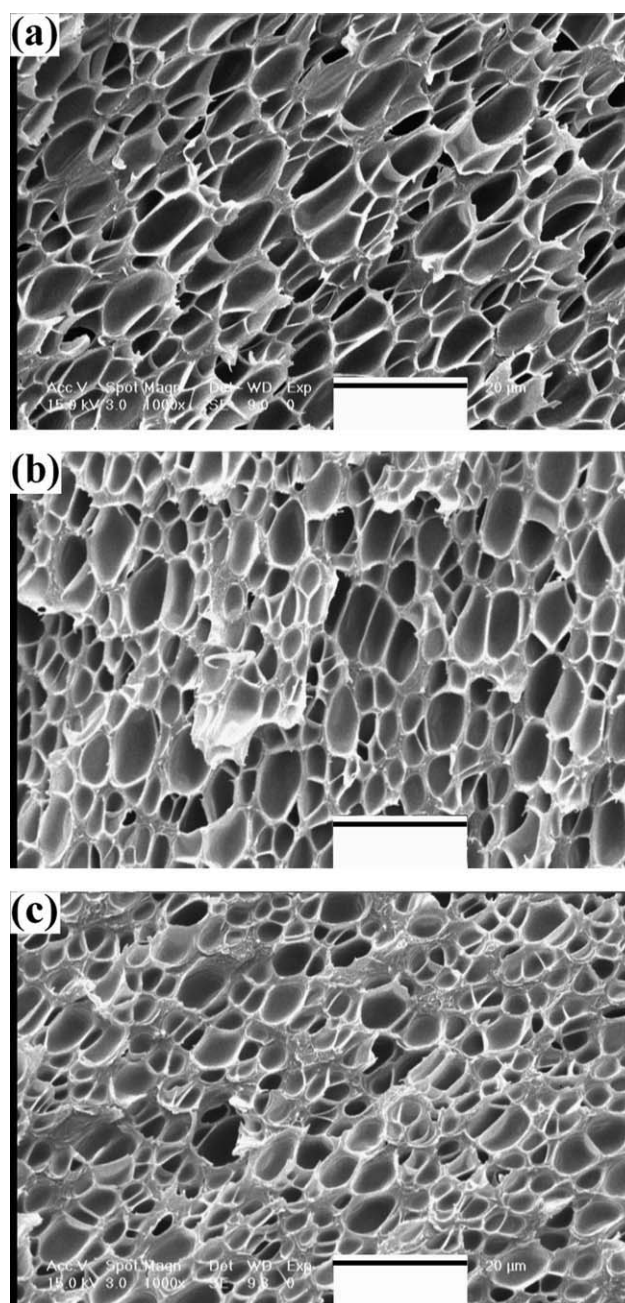

Figure 6 SEM micrographs of (a) $PSNS_{150}N_1$, (b) $PSNS_{150}N_2$, and (c) $PSNS_{150}N_3$. The scale bars are equal to 20 μm.

predicted by classical nucleation theory. This is a result of the special features of the foaming process used in this study. As previously explained in more detail,[20] preservation of the primary induced structures in the initial stages of the foaming process via increases in the nucleation rate and via control of bubble coalescence and gas escape from the polymer matrix makes the nucleation of bubbles the dominant mechanism determining the final cellular structure.

TABLE V
Cell Densities and Nucleation Ratios of the PSNS$_{200}$ and PSNS$_{150}$ Nanocomposites

Nanocomposite type	Nanocomposite name	Cell density mean (number/cm^3)	Standard deviation	Nucleation ratio[a]
PSNS$_{150}$	PSNS$_{150}$N$_1$	1.83×10^{11}	3.12×10^{10}	29
	PSNS$_{150}$N$_2$	2.31×10^{11}	5.50×10^{10}	37
	PSNS$_{150}$N$_3$	3.70×10^{11}	2.5×10^{10}	59
PSNS$_{200}$	PSNS$_{200}$N$_1$	2.55×10^{11}	9.74×10^{10}	41
	PSNS$_{200}$N$_2$	3.49×10^{11}	1.31×10^{11}	56
	PSNS$_{200}$N$_3$	12.4×10^{11}	1.2×10^{11}	66

[a] N_0 was 6.2×10^9.

CONCLUSIONS

The controlled fabrication of desired cellular structures makes it necessary to gain comprehensive knowledge of the variables affecting the process. In this study, we considered the properties of nanoparticles as effective parameters, but the quality of their effects is partially vague.

Generally, we observed that with the nanoparticle content increasing, the cell density of the final foam increased. We also showed that nucleation was performed by nanosilica particles acting as nucleating agents, and heterogeneous nucleation was the dominant mechanism.

The morphological characteristics of the nanocomposite foams included smaller sizes and bimodal distributions of the cell sizes.

The results showed that nanosilicas of larger sizes could result in foams with higher cell densities. Additionally, the cell density of the foams could be reduced by increases in the chemical affinity between the surfaces of the nanoparticles and the polymer matrix. These results agree with the effects of nucleation agent characteristics on the nucleation of bubbles, as reported previously.[29]

References

1. Handa, Y. P.; Liao, X.; Yoshitaka, Y.; Tomohiro, M. Polym Int 2007, 56, 67.
2. Krause, B.; Mettinkhof, R.; Van der Vegt, N. F. A.; Wessling, M. Macromolecules 2001, 34, 874.
3. Krause, B.; Diekmann, K.; Van der Vegt, N. F. A.; Wessling, M. Macromolecules 2002, 35, 1738.
4. Tomasko, D. L.; Han, X.; Liu, D.; Gao, W. Curr Opin Solid State Mater Sci 2003, 7, 407.
5. Lee, L. J.; Zeng, C. X.; Cao, X.; Han, J.; Shen, X. G. Compos Sci Technol 2005, 65, 2344.
6. Siripurapu, S.; DeSimone, J. M.; Khan, S. A.; Spontak, R. J. Macromolecules 2005, 38, 227.
7. Shen, J.; Zeng, C.; Lee, L. J. Polymer 2005, 46, 5218.
8. Ema, Y.; Ikeya, M.; Okamoto, M. Polymer 2006, 47, 5350.
9. Han, X.; Shen, J.; Huang, H.; Tomasko, D. L.; Lee, L. J. Polym Eng Sci 2007, 48, 103.
10. Zeng, C.; Han, X.; Lee, L. J.; Koelling, K. W.; Tomasko, D. L. Adv Mater 2003, 15, 1743.
11. Han, X.; Zeng, C.; Lee, L. J.; Koelling, K. W.; Tomasko, D. L. Polym Eng Sci 2003, 43, 1261.
12. Lee, M.; Lee, B.; Choi, K. World Pat. 2004074357 (2004).
13. Di, Y.; Iannace, S.; Maio, E. D.; Nicolais, L. J Polym Sci Part B: Polym Phys 2005, 43, 689.
14. Krause, B.; Koops, G. H.; Van der Vegt, N. F. A.; Wessling, M.; Wubbenhorst, M. Presented at the 7th International Conference on Solid Dielectrics, Eindhoven, the Netherlands, June 25–29, 2001.
15. Prathamesh, D.; Sindee, S. Polym Eng Sci 2005, 43, 640.
16. Yokoyama, H.; Sugiyama, K. Macromolecules 2005, 38, 10516.
17. Yokoyama, H.; Li, L.; Nemoto, T.; Sugiyama, K. Adv Mater 2004, 16, 1542.
18. DeSimone, J. M.; Siripurapu, S.; Khan, S. A.; Spontak, R. J.; Royer, J. U.S. Pat. 0168509 (2002).
19. Hedrick, J. L.; Russel, T. P.; Hedrick, J. C.; Hilborn, J. G. J Polym Sci Part A: Polym Chem 1996, 34, 2879.
20. Janani, H.; Famili, M. H. N. Polym Eng Sci, to appear.
21. Colton, J. S.; Suh, N. P. Polym Eng Sci 1987, 27, 493.
22. Colton, J. S.; Suh, N. P. Polym Eng Sci 1987, 27, 500.
23. Shen, J.; Zeng, C.; Lee, L. J. Polymer 2005, 46, 5218.
24. Goren, K.; Chen, L.; Schadler, L. S.; Ozisik, R. J Supercrit Fluids 2010, 51, 420.
25. Saha, M. C.; Kabir, M. E.; Jeelani, S. Mater Sci Eng A 2008, 479, 213.
26. Hwang, S.; Hsu, P. P.; Yeh, J.; Yang, J.; Chang, K.; Lai, Y. Int Commun Heat Mass Transfer 2009, 36, 471.
27. Colton, J. S. Ph.D. Thesis, Massachusetts Institute of Technology, 1985.
28. Joshi, K.; Lee, J. G.; Shafi, M. A.; Flumerfelt, R. W. J Appl Polym Sci 1998, 57, 1353.
29. Fletcher, N. H. J Chem Phys 1958, 29, 572.
30. Chen, C. U.S. Pat. 0245665 (2005).
31. Kumar, V.; Suh, N. Polym Eng Sci 1990, 30, 1323.